Regulation of myocardial substrate metabolism during increased energy expenditure: insights from computational studies

Lufang Zhou, Marco E. Cabrera, Isidore C. Okere, Naveen Sharma and William C. Stanley

Am J Physiol Heart Circ Physiol 291:1036-1046, 2006. First published Apr 7, 2006;
doi:10.1152/ajpheart.01382.2005

AJP - Heart and Circulatory Physiology publishes original investigations on the physiology of the heart, blood vessels, and lymphatics, including experimental and theoretical studies of cardiovascular function at all levels of organization ranging from the intact animal to the cellular, subcellular, and molecular levels. It is published 12 times a year (monthly) by the American Physiological Society, 9650 Rockville Pike, Bethesda MD 20814-3991. ISSN: 0363-6135, ESSN: 1522-1539. Visit our website at http://www.the-aps.org/.

Am J Physiol Heart Circ Physiol 291: H1036–H1046, 2006.
First published April 21, 2006; doi:10.1152/ajpheart.01382.2005.

Regulation of myocardial substrate metabolism during increased energy expenditure: insights from computational studies

Lufang Zhou,[1,5] Marco E. Cabrera,[1,2,3,5] Isidore C. Okere,[2,5] Naveen Sharma,[4,5] and William C. Stanley[2,4,5]

Departments of Biomedical Engineering,[1] Physiology and Biophysics,[2] Pediatrics,[3] Nutrition,[4] and the Center for Modeling Integrated Metabolic Systems,[5] Case Western Reserve University, Cleveland, Ohio

Submitted 29 December 2005; accepted in final form 27 March 2006

Zhou, Lufang, Marco E. Cabrera, Isidore C. Okere, Naveen Sharma, and William C. Stanley. Regulation of myocardial substrate metabolism during increased energy expenditure: insights from computational studies. *Am J Physiol Heart Circ Physiol* 291: H1036–H1046, 2006. First published April 21, 2006; doi:10.1152/ajpheart.01382.2005.—In response to exercise, the heart increases its metabolic rate severalfold while maintaining energy species (e.g., ATP, ADP, and Pi) concentrations constant; however, the mechanisms that regulate this response are unclear. Limited experimental studies show that the classic regulatory species NADH and NAD^+ are also maintained nearly constant with increased cardiac power generation, but current measurements lump the cytosol and mitochondria and do not provide dynamic information during the early phase of the transition from low to high work states. In the present study, we modified our previously published computational model of cardiac metabolism by incorporating parallel activation of ATP hydrolysis, glycolysis, mitochondrial dehydrogenases, the electron transport chain, and oxidative phosphorylation, and simulated the metabolic responses of the heart to an abrupt increase in energy expenditure. Model simulations showed that myocardial oxygen consumption, pyruvate oxidation, fatty acids oxidation, and ATP generation were all increased with increased energy expenditure, whereas ATP and ADP remained constant. Both cytosolic and mitochondrial NADH/NAD^+ increased during the first minutes (by 40% and 20%, respectively) and returned to the resting values by 10–15 min. Furthermore, model simulations showed that an altered substrate selection, induced by either elevated arterial lactate or diabetic conditions, affected cytosolic NADH/NAD^+ but had minimal effects on the mitochondrial NADH/NAD^+, myocardial oxygen consumption, or ATP production. In conclusion, these results support the concept of parallel activation of metabolic processes generating reducing equivalents during an abrupt increase in cardiac energy expenditure and suggest there is a transient increase in the mitochondrial NADH/NAD^+ ratio that is independent of substrate supply.

diabetes; exercise; heart; lactate; mitochondria; modeling

CARDIAC PUMP FUNCTION is fueled by ATP hydrolysis, which is precisely matched by ATP formation, primarily in the mitochondria (42). In the transition from rest to intense exercise, there is a three- to sixfold increase in the rate of cardiac power generation, myocardial oxygen consumption ($M\dot{V}O_2$), and ATP turnover (25). Nevertheless, at high work states the myocardial ATP and ADP concentrations are maintained at a relatively constant level (2, 4, 36). There is rapid activation of NADH generation in the mitochondria, flux through the electron transport chain (ETC), and ATP production by oxidative phosphorylation to match exactly ATP breakdown in the cytosol. Studies in isolated mitochondria show that the generation of NADH from carbon substrates, oxygen consumption, and oxidative phosphorylation are turned on by feedback from an increase in ADP concentration (9); however, the regulatory mechanisms in vivo are still unclear. Experimental studies suggest that the mitochondrial NADH and NAD^+ are also maintained near steady-state values at high rates of energy expenditure due to the matching of NADH oxidation by complex I of the ETC with the rapid activation of substrate metabolism and NADH formation by dehydrogenases [e.g., pyruvate dehydrogenase (PDH), fatty acids oxidation, and the Krebs tricarboxylic acid cycle] (22, 36). The stability of these regulatory species in the heart demonstrate that metabolic control models based solely on changes in the levels of these intermediates to control metabolic flux rates cannot fully explain the observed responses (5, 27–29).

An alternative regulatory hypothesis proposes that there is simultaneous parallel activation of ATP utilization and production, glycolysis, and mitochondrial dehydrogenases by signaling molecules, e.g., Ca^{2+} (6, 7, 31, 43). Simulations from an integrated computational model of cardiac mitochondrial energy metabolism demonstrate that an increase in Ca^{2+} concentration in the mitochondrial matrix activates NADH generation and oxidative phosphorylation (13). Indeed, Korzeniewski et al. (27–29) found additional support for the parallel-activation mechanism in the skeletal muscle and the heart by using a dynamic computer model of oxidative phosphorylation; however, this model did not incorporate metabolic pathways for substrate metabolism and NADH generation. Because current experimental measurements of myocardial metabolism lump the cytosol and mitochondria, it is important to distinguish these subcellular compartments in computational models to provide better insight into the metabolic responses during the transition to increase cardiac power.

The plasma concentration of substrates effect the metabolic response to increased cardiac work such as with the rise in arterial lactate concentration during physical exercise. Myocardial lactate uptake during exercise is increased as a function of the arterial lactate concentration (16, 23, 38), which is dependent on the rate of systemic lactate production and clearance (39). In addition, studies in resting dogs (37) and perfused rat hearts (15) demonstrate that an elevation in arterial lactate concentration reduces the relative contribution of fatty acids to $M\dot{V}O_2$ (37). The mechanism for this effect is not clear but could be due to a lactate-induced increase in cytosolic and/or

Address for reprint requests and other correspondence: W. C. Stanley, Dept. of Physiology and Biophysics, School of Medicine, Case Western Reserve Univ., 10900 Euclid Ave., Cleveland, OH 44106-4970 (e-mail: wcs4@case.edu).

The costs of publication of this article were defrayed in part by the payment of page charges. The article must therefore be hereby marked "*advertisement*" in accordance with 18 U.S.C. Section 1734 solely to indicate this fact.

mitochondrial NADH/NAD$^+$ and inhibition of mitochondrial fatty acid oxidation through NADH inhibition of β-oxidation. Plasma substrate levels are also altered with diabetes, as are the expression and activity of key enzymes and transporters. The metabolic adaptations to diabetes are particularly complex because there is both altered substrate availability (e.g., increased plasma ketone bodies and glucose) and altered expression of key proteins (e.g., phosphofructokinase, pyruvate dehydrogenase kinase, and glucose transporters) that effect myocardial substrate selection. During increased cardiac power we observed that diabetic pigs have decreased PDH activity and lactate uptake and enhanced β-hydroxybutyrate uptake compared with healthy animals (19). It is generally postulated that impaired pyruvate oxidation in the diabetic heart is partially due to an increase in mitochondrial NADH/NAD$^+$ (19, 32, 33, 40); however, evidence for this is lacking due to the inability to measure mitochondrial NADH and NAD$^+$ in the intact heart.

The overall goal of the present study was to *1*) assess the role of parallel activation of multiple metabolic steps in the regulation of cytosolic and mitochondrial NADH/NAD$^+$ during the dynamic transition from resting conditions to high rates of cardiac energy expenditure, as observed with exercise; *2*) investigate the effects of elevated arterial lactate concentration on mitochondrial pyruvate and fatty acid oxidation and the cytosolic and mitochondrial NADH/NAD$^+$ ratios; and *3*) determine whether impaired pyruvate oxidation under diabetic conditions requires an increase in mitochondrial NADH/NAD$^+$. We modified our recently published computational model of cardiac metabolism (8, 46, 47) by incorporating multistep activation mechanisms (29) and simulated the metabolic responses of the heart to an abrupt increase in energy expenditure. We hypothesized that in response to an abrupt increased cardiac energy expenditure, the simultaneous activation of ATP hydrolysis, ATP synthesis, glycogen breakdown, NADH generation, and electron transport chain activity would maintain constant ATP and ADP levels but cause a sharp increase in the cytosolic NADH/NAD$^+$ ratio, with less effect on mitochondrial NADH/NAD$^+$. On the other hand, elevation in arterial lactate concentration simultaneously with the increase in energy expenditure would increase the cytosolic NADH/NAD$^+$ ratio and mitochondrial pyruvate oxidation and reduce fatty acid oxidation, with little effect on mitochondrial NADH/NAD$^+$ ratio. Finally, we hypothesized that simulation of diabetic conditions would reduce pyruvate oxidation but would not require an increase in mitochondrial NADH/NAD$^+$.

METHODS

Model development. To quantitatively investigate the effects of increased energy expenditure on cardiac energy metabolism and potential regulatory mechanisms, we modified our previously published cardiac model of ischemia (48) by including multistep activation of specific metabolic processes. As in our ischemia model (47,

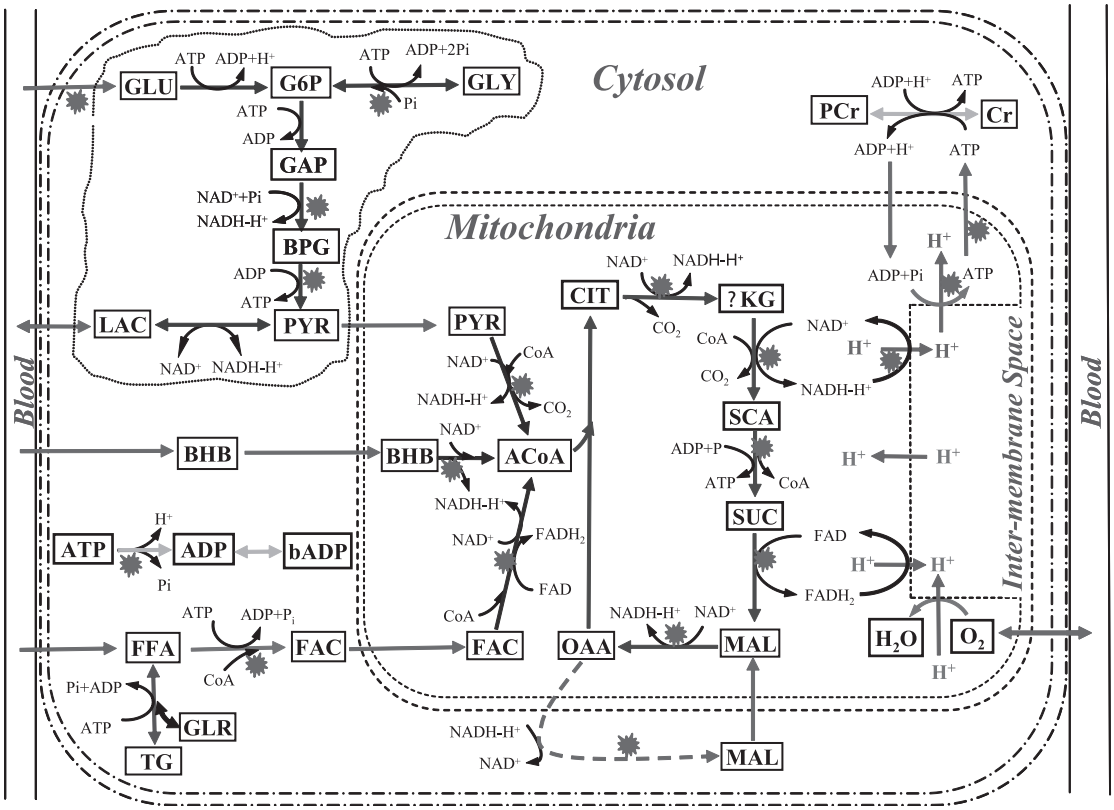

Fig. 1. Myocardium metabolic pathway. This complex network incorporates most key biochemical reactions and pathways involved in cardiac metabolism, including glycolysis, pyruvate oxidation, fatty oxidation, the tricarboxylic acid cycle, and oxidative phosphorylation. It also includes species transport across cellular membrane and mitochondrial membrane, as well as proton influx and efflux between mitochondrial matrix and inter-membrane space. GLU, glucose; G6P, glucose-6-phosphate; GLY, glycogen; GAP, glyceraldyhe-3-phosphate; BPG, 1,3-bisphosphate-glycerate; PYR, pyruvate; LAC, lactate; TG, triglyceride; GLR, glycerol; FFA, free FA; FAC, fatty acyl-CoA; PCr, phosphocreatine; Cr, creatine; CIT, citrate; α-KG, α-ketoglutarate; SCA, succinyl-CoA; SUC, succinate; MAL, malate; OAA, oxaloacetate; ACoA, acetyl-CoA; bADP, bound ADP; ADP, free ADP; BHB, β-hydroxybutyrate. *Activation of metabolic process with onset of increase energy expenditure.

48), the dynamic mass balance equation for species j in a spatially lumped capillary blood domain (accounting for fractional mixing between the arterial and venous blood) was described as:

$$V_b \frac{dC_{bj}}{dt} = \frac{Q(C_{aj} - C_{bj})}{F} - J_{b-c,j} \quad (1)$$

where C_{aj} is the arterial concentration of species j, C_{bj} is the blood concentration, V_b is the domain volume, Q is blood flow, $0 < F \leq 1$ is the mixing factor, and $J_{b\text{-}c,j}$ is the mass transport rate between blood and cytosol.

The dynamic mass balance of species j in the spatially lumped cytosolic domain was described by the involved metabolic reactions in the domain and mass transfer across the cellular membrane and mitochondrial membrane:

$$V_{cj} \frac{dC_{cj}}{dt} = R_{cj} + J_{b-c,j} - J_{c-m,j} \quad (2)$$

where C_{cj} is the concentration, V_{cj} is the effective volume of species j in the cytosol, R_{cj} is the metabolic reaction rate of species j, and $J_{c-m,j}$ is the mass transport rate between cytosol and mitochondria.

In the mitochondrial domain, the dynamic mass balance equation for species j is

$$V_{mj} \frac{dC_{mj}}{dt} = R_{mj} + J_{c-m,j} \quad (3)$$

where C_{mj} is the concentration, V_{mj} is the effective volume of species j in the mitochondrial domain, and R_{mj} is the net reaction rate.

The dynamic mass balance for protons in the mitochondrial intermembrane space is

$$V_i \frac{dC_{i,H}}{dt} = J^f_{m\to i,H} - J^f_{i\to m,H} - J_{\text{Hleak}} \quad (4)$$

where V_i is the effective volume of intermembrane space, $J^f_{m\to i,H}$ is the proton efflux from mitochondrial matrix to intermembrane space, $J^f_{i\to m,H}$ is the proton influx, and J_{leak} is the proton leak flux through the mitochondrial inner membrane. The proton fluxes values under steady state and the corresponding parameters can be found in our recently published paper (47).

The reaction and transport kinetics terms in the mass balance equations (e.g., glycolysis, oxygen consumption, ATP synthesis, glucose uptake, etc.) were described by Michaelis-Menten equations as in our ischemia model. To simulate increased energy demand in the model of cardiac cellular metabolism, we assumed simultaneous activations of multistep metabolic fluxes in both cytosol and mitochondria (Fig. 1), as well as increase in myocardial blood flow (MBF). Consequently, simultaneous activation occurred with glucose uptake, glycogen breakdown, glycolysis, ATP hydrolysis, dehydrogenase, Krebs tricarboxylic acid cycle, oxygen consumption (complex I), and ATP synthesis (complex V) (35). This activation was implemented in the model by increasing the maximal velocity (V_{max}) of metabolic fluxes n times through the Michaelis-Menten coefficients for corresponding processes that are proportional to the increase in energy expenditure:

$$V'_{x-y,v-w} = n \times V_{x-y,v-w} \quad (5)$$

The results of this multistep activation mechanism will be evident in model simulations, which correspond closely with published experimental data in pigs (36) involving oxygen consumption, glucose oxidation, and fatty acid oxidation with increased cardiac work induced by a simultaneous injection of atropine, infusion of dobutamine, and constriction of the proximal thoracic aorta.

To simulate the dynamic responses of the diabetic heart to increased energy expenditure, we incorporated β-hydroxybutyrate in the present model (Fig. 1) because in the diabetic heart, there is an elevated uptake and oxidation of ketone bodies (primarily β-hydroxybutyrate), which is concentration dependent (19, 41). We assumed that the concentration of β-hydroxybutyrate under normal conditions is very low, and it increases with diabetes, therefore, the rate of β-hydroxybutyrate oxidation increases.

Parameter estimation and simulation strategy. The initial values of the reaction flux rates, transport flux rates, and species concentrations of this model were modified so that they matched the published experimental values collected in pigs during the baseline period (26, 36). The species concentrations (in the blood, cytosol, and mitochondria) were obtained by taking into account the relative distribution of these species in the specific subcellular domains as in our previous models and are listed in Table 1. Values for the reaction and transport rates and associated parameter values that were updated in this model are listed in Tables 2 and 3; the remainder of the parameter values were the same as in our previously published model (8, 46, 47).

Simulations were oriented to investigate the metabolic responses and the regulation of metabolic processes in the cytosol and mitochondria during the transition from resting to conditions of a fourfold exponential increase ($\tau = 0.3$ min) in energy expenditure and MBF. These simulations emphasized the time profiles of key metabolite concentrations (e.g., ATP, ADP, NADH, NAD^+, glycogen, lactate, etc.) and metabolic fluxes (e.g., oxygen consumption, glycolysis, ATP hydrolysis, FAO, etc.) and were compared with previously published experimental data in pigs. The model was then used to simulate the metabolic responses of the heart to the increased energy expenditure under different metabolic milieus: *1*) constant arterial levels of substrates [reflecting the baseline conditions in our recent studies in anesthetized pigs (26, 36)]; *2*) elevated arterial lactate concentrations [0.7 mM (normal), 2.1 mM, and 4.2 mM] initiated with the onset of increased myocardial energy expenditure; and *3*) diabetic conditions (high β-hydroxybutyrate + high arterial glucose + inhibited glucose

Table 1. *Species concentration in blood, cytosol, and mitochondria*

Species	Blood and Interstitial Fluid Domain, mM	Cytosolic Domain, μmol/g wet wt	Mitochondrial Domain, μmol/g wet wt
GLU	4.65	0.56	
G6P		0.17	
GLY		36.0*	
GAP		0.014	
BPG		0.04	
PYR	0.068	0.2	0.2
LAC	0.6	2.6*	
TG		4.27	
GLR		0.015	
FFA	0.44	0.022	
FAC		8.4×10^{-3}	0.048
CoA		2.0×10^{-3}	0.069
PCr		11.8	0
Cr		5	0
NAD		0.07*	2.14
NADH		3.5×10^{-3}*	0.51
ATP		4.5	1.61
ADP		0.051	2
bADP		1.51	
AMP		2.5×10^{-4}	
Pi		1.89	20
OAA		1.0×10^{-3}	0.017
MAL		0.012	0.94
ACoA		1.3×10^{-3}	1.6×10^{-3}
CIT		0.042	3.39
aKG		2.0×10^{-3}	0.17
SCA			0.033
SUC			1.26
O2	4.03	0.96	0.96
CO2	17.27	20.0	20.0

*Data from Sharma et al. (36).

Table 2. *Reactions fluxes and parameter values under normal steady-state condition*

Reactions	Flux Values, μmol·min^{-1}·(g^{-1}·wet wt)$^{-1}$	Parameters			
		$V_{x\text{-}y,v\text{-}w}$	$K_{x\text{-}y,v\text{-}w}$	$\mu^{\pm}$	$v^{\pm}$
$\Phi_{GLU,G6p}$	0.12	1.92	8.4	0.088 (+)	0
$\Phi_{G6P,GLY}$	0.2	0.40	0.17	180 (+)*	0
$\Phi_{GLY\text{-}Pi,G6P}$	0.2	3.0	953	5.6×10^{-7} (−)*	0
$\Phi_{G6P,GAP}$	0.12	1.21	1.54	5.6×10^{-7} (+)	0
$\Phi_{GAP,BGP}$	0.24	28.8	0.13	0	380 (−)
$\Phi_{BPG,PRY}$	0.24	7.68	0.6	1.1×10^{-2} (−)	0
$\Phi_{PYR,LAC}$	0.13	1.57	2	0	5×10^{-3} (+)
$\Phi_{LAC,PYR}$	0.25	0.34	0.78	0	0.2 (−)
$\Phi_{PYR\text{-}CoA,ACoA}$	0.37	8.03	1.4×10^{-2}	0	41.96 (−)
$\Phi_{TG,GLR}$	0.02	0.04	4.27	0	0
$\Phi_{GLR\text{-}FFA,TG}$	0.06	0.06	3.3×10^{-6}	0.088 (+)	0
$\Phi_{FA\text{-}CoA,FAC}$	0.07	0.78	1.5×10^{-2}	0.88 (+)	0
$\Phi_{FAC\text{-}CoA,ACoA}$	0.07	1.69	3.0×10^{-4}	0	42 (−) 8.8 (−)†
$\Phi_{ACoA,CIT}$	0.93	22.2	3.1×10^{-4}	0	0
$\Phi_{CIT,aKG}$	0.93	11.1	7.26	0	8.39 (−)
$\Phi_{aKG\text{-}CoA,SCA}$	0.93	11.1	0.51	0	8.39 (−)
$\Phi_{SCA,SUC}$	0.93	3.77	9.9×10^{-2}	0.025 (−)	0
$\Phi_{SUC,MAL}$	0.93	11.1	3.78	0	17.7 (−)†
$\Phi_{MAL,OAA}$	0.93	11.1	2.82	0	8.39 (+)
$\Phi_{PCR,CR}$	2.42	40.0	165.2	1.1×10^{-3} (−)	0
$\Phi_{CR,PCR}$	2.42	40.0	70	8.82 (+)	0
$\Phi_{ADP,bADP}$	10	11.0	5.1×10^{-3}	0	0
$\Phi_{bADP,ADP}$	10	1.01×10^{3}	151	0	0
$\Phi_{AMP,ADP}$	1.82	404	2.5×10^{-3}	88.2	0
$\Phi_{ADP,AMP}$	1.82	44.0	0.51	0.011	0
$\Phi_{O2,H2O,N}$	2.0	43.9	9.6×10^{-2}	0	4.53 (+)
$\Phi_{ATP,ADP}$	15.6	1.59×10^{3}	8.7×10^{3}	0	0
$\Phi_{O2,H2O,F}$	0.71	15.67	9.6×10^{-2}	0	2.16 (+)†
$\Phi_{ADP,ATP}$	14.8	3.58×10^{2}	0	23.6	$(PG)_0 = 123$

ϕ, reaction flux. See text for abbreviations. C_{ATP}/C_{ADP} (μ) or C_{NADH}/C_{NAD} (ν) is controller; (−), C_{ADP}/C_{ATP} (μ) or C_{NAD}/C_{NADH} (ν) is controller; *C_{AMP}/C_{ATP} or C_{ATP}/C_{AMP} is controller; †C_{FADH2}/C_{FAD} or C_{FAD}/C_{FADH2} is controller; $V_{x-y,v-w}$, maximal reaction rate (μmol·min^{-1}·g·$^{-1}$); $K_{x-y,v-w}$, reaction coefficient (μmol/g.wet wt).

uptake). Computer simulations were obtained by solving the model equations by using DLSODE, a robust implicit integrator for stiff and sparse systems (CASC, 2003; http://www.llnl.gov/CASC/odepack/software/dlsode.f).

SIMULATION RESULTS

Elevated metabolic fluxes during increased energy expenditure. With the increase of cardiac ATP hydrolysis, there were significant and immediate increases in $M\dot{V}O_2$ and ATP generation through oxidative phosphorylation (Fig. 2). $M\dot{V}O_2$ increased 3.8-fold (from 2.7 to 10.1 μmol·g^{-1}·min^{-1}) and then decreased slightly to 9.9 μmol·g^{-1}·min^{-1} at 15 min. Consistent with increased $M\dot{V}O_2$, ATP generation rate increased approximately fourfold from 14.8 to 58.8 μmol·g^{-1}·min^{-1} and then decreased to 57.5 μmol·g^{-1}·min^{-1}. ATP hydrolysis rate dynamics followed similar pattern (increased from 15.6 to

Table 3. *Transport rates and model parameter values under normal, resting steady state*

Species	Flux Value, μmol·min^{-1}·(g^{-1}·wet wt)$^{-1}$	Parameters
GLU	$J^{f}_{b\to c,GLU} = 0.12$	$M_{b\to c,GLU} = 4$*, $T_{b\to c,GLU} = 0.22$
LAC	$J^{f}_{b\to c,LAC} = 0.53$	$M_{b\to c,LAC} = 6.0$*, $T_{b\to b,LAC} = 5.33$
	$J^{f}_{b\to b,Lac} = 0.41$	$M_{c\to b,LAC} = 0.026$, $T_{c\to b,LAC} = 0.41$
PYR	$J^{f}_{c\to m,PYR} = 0.37$	$M_{c\to m,PYR} = 2.0$, $T_{c\to m,PYR} = 8.03$
FFA	$J^{p}_{b\leftrightarrow c,FFA} = 0.07$	$\sigma_{b\leftrightarrow c,FFA} = 17.4$, $\lambda_{b\leftrightarrow c,FFA} = 1.14$
FAC	$J^{f}_{c\to m,FAC} = 0.07$	$M_{c\to m,FAC} = 0.0084$, $T_{c\to m,FAC} = 0.14$
O_2	$J^{p}_{b\leftrightarrow c,O2} = 2.70$	$\sigma_{b\leftrightarrow c,O_2} = 3.25$, $\lambda_{b\leftrightarrow c,O_2} = 2.98$
Co_2	$J^{p}_{b\leftrightarrow c,CO2} = 2.22$	$\sigma_{b\leftrightarrow c,CO_2} = 1.0$, $\lambda_{b\leftrightarrow c,CO_2} = 0.81$
ATP†	$J^{f}_{m\to c,ATP} = 15.74$	$M_{m\to c,ATP} = 40.25$, $T_{m\to c,ATP} = 0.8 \times 10^{3}$
M-A shuttle‡	$J^{f}_{c\to m,NADH} = 0.37$	$M_{m\to c,NAD} = 41.96$, $T_{a\to m,NADH} = 20.08$
		$M_{c\to m,NADH} = 0.2$
H leakage	$J^{leakage}_{a\to m,H} = 4.0$	$M^{leakage}_{a\to m,H} = 123.01$, $T^{leakage}_{a\to m,H} = 2.00$

J, transport rate (μmol·min^{-1}·g wet wt^{-1}) *M, affinity coefficient (μmol/g·wet wt) or mM; T, normalized transport rate coefficient (μmol·min^{-1}·g·wet wt^{-1}); λ, membrane permeability coefficient (min^{-1}); σ, partition coefficient; †transport flux and parameter of P_1 and ADP were assumed to be same as that of ATP; ‡M-A shuttle was described as $J^{f}_{c\to m,NADH} = T_{c\to m,NADH}\left[\frac{RS^{+}_{c}}{M_{c\to m,NADH} + RS^{+}_{c}}\right]\left[\frac{RS^{-}_{m,N}}{M_{m\to c,NAD} + RS^{-}_{m,N}}\right]$.

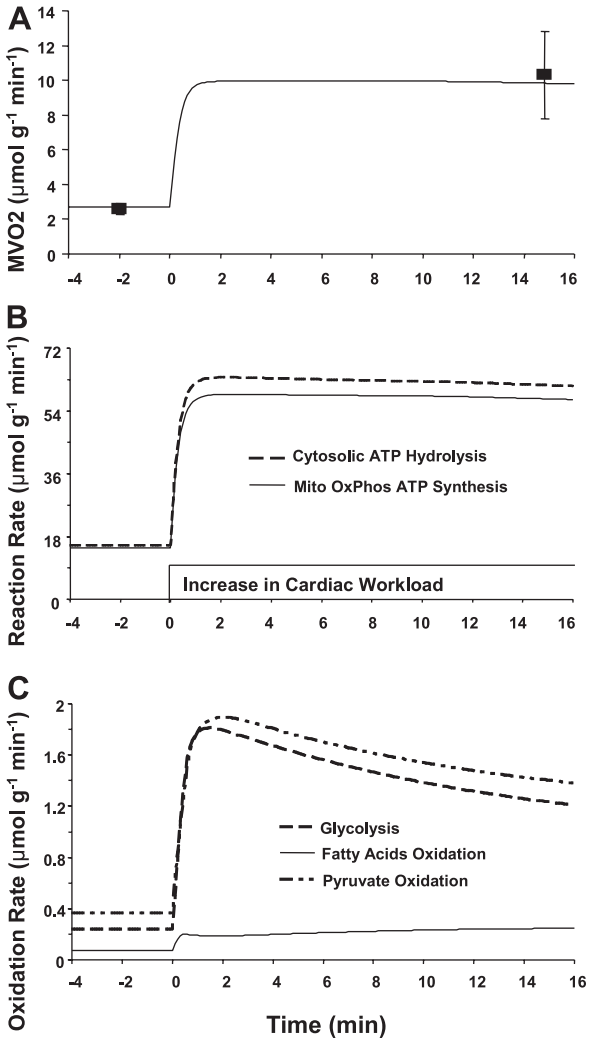

Fig. 2. Model simulated dynamics of myocardial O_2 consumption ($M\dot{V}O_2$) (*A*), ATP hydrolysis and ATP generation by oxidative phosphorylation (*B*), and glycolysis, pyruvate oxidation, and fatty acid oxidation (*C*) in response to a fourfold increased energy expenditure. Solid squares represent experimental data on $M\dot{V}O_2$ from pig experiments (from Ref. 36).

63.7 μmol·g^{-1}·min^{-1} then decreased to 61.4 μmol·g^{-1}·min^{-1}) in response to increased cardiac energy expenditure.

The increase in energy expenditure also stimulated glycolysis, pyruvate oxidation, and β-oxidation (Fig. 2). The glycolytic rate increased from its resting state value of 0.12 μmol·g^{-1}·min^{-1} to a peak value of 0.91 μmol·g^{-1}·min^{-1} (7.6-fold) then decreased to 0.63 μmol·g^{-1}·min^{-1} (5.3-fold) as glycogen was depleted (Fig. 2*C*). The pyruvate oxidation rate increased to a peak value of 1.88 μmol·g^{-1}·min^{-1} and then decreased to 1.38 μmol μmol·g^{-1}·min^{-1} (Fig. 2*C*). Fatty acid β-oxidation increased from 0.07 to 0.24 μmol·g^{-1}·min^{-1}at 15 min of increased energy expenditure (Fig. 2*C*).

Species concentration dynamics in response to increased cardiac energy expenditure. The myocardial glycogen concentration decreased exponentially from its initial value of 36 to 15.9 μmol/g at 15 min of increased energy expenditure, whereas the lactate concentration increased from 2.6 to 5.9 μmol/g (Fig. 3*A*). Although the ATP concentration in the mitochondria slightly decreased, the cytosolic ATP concentration remained constant (Fig. 3).

There was a small transient increase in NADH and decrease in NAD^+ in both the cytosol and mitochondria. The changes were greater in the cytosolic than in the mitochondrial compartment, with the peak increase in the NADH/NAD^+ ratio being a 40% increase in the cytosol and 20% in the mitochondria, with a return to baseline values by 15 min of increased cardiac energy expenditure (Fig. 4). To compare simulation results with experimental data, we calculated the tissue NADH and NAD^+ concentrations from their cytosolic and mitochondrial values assuming the volume ratio of cytosol to mitochondria to be 70:17 (46). The result shows that the simulated tissue NADH and NAD^+ concentrations and NADH/NAD^+ ratio matched the tissue measurements made at 15 min of increased cardiac energy expenditure; however, sampling late in the stimulation period missed the predicted transient increase in NADH/NAD^+ ratio at the onset of increased cardiac energy expenditure (Fig. 4*C*).

Effects of pathway activation on metabolic homeostasis. The mechanisms responsible for the maintenance of regulatory species (high-energy phosphates and nicotinamide adenine dinucleotides) were further investigated by systematically

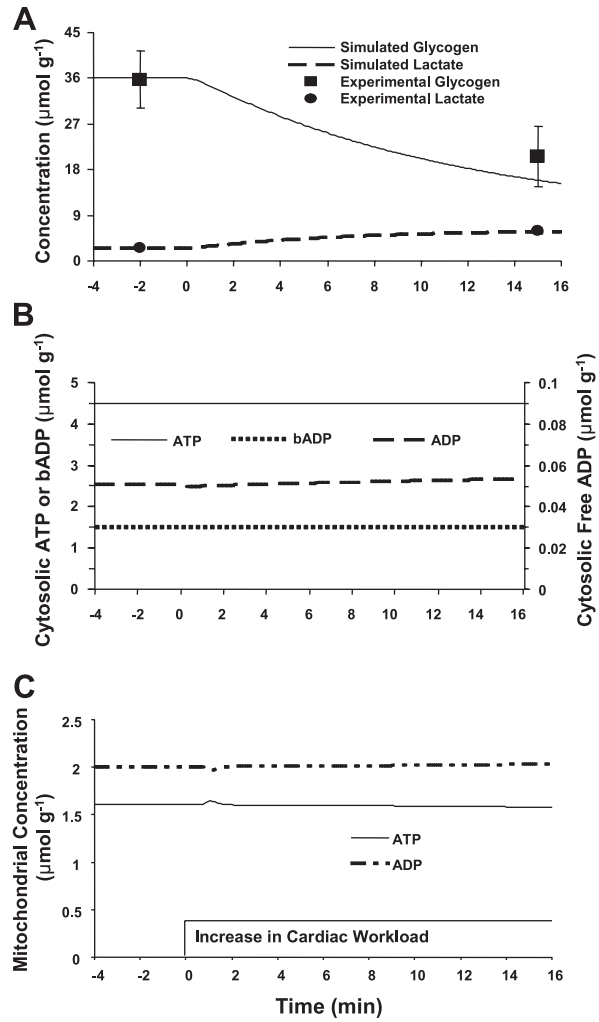

Fig. 3. Model simulated dynamics of glycogen and lactate (*A*), cytosolic ATP and ADP (*B*), and mitochondrial ATP and ADP (*C*) concentrations in response to fourfold increased energy expenditure. Solid circles and squares represent experimental data on lactate and glycogen concentrations, respectively.

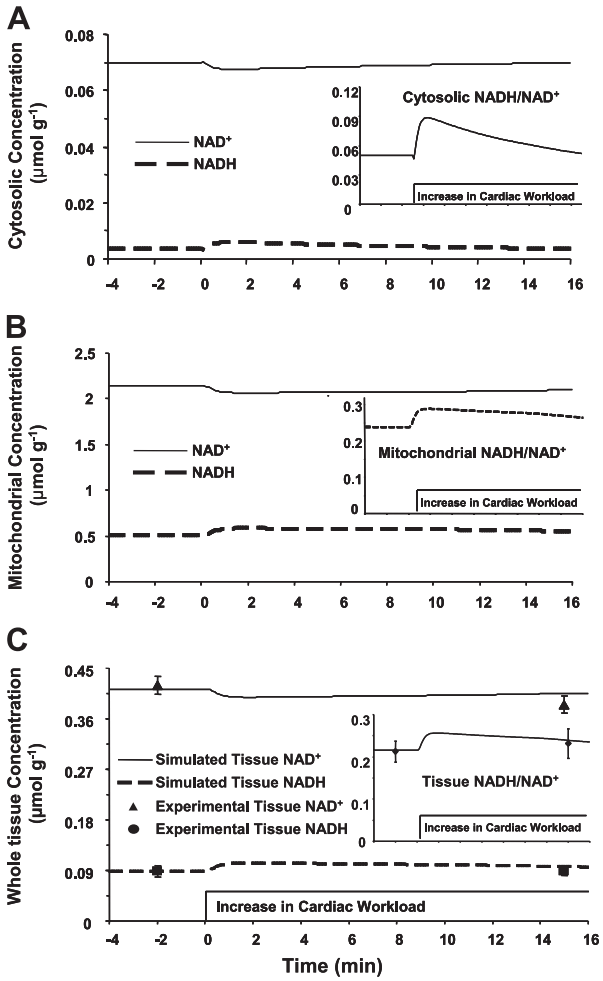

Fig. 4. Model simulated dynamics of NADH and NAD^+ concentrations in the cytosol (*A*), mitochondria (*B*), and whole tissue (*C*) in response to increased energy expenditure. Solid triangle and circles represent experimental data on tissue NAD^+ and NADH concentrations, respectively. *Insets*: $NADH/NAD^+$ ratios plotted on the same time scale.

eliminating the activation of specific metabolic processes with the increase in cardiac energy expenditure (Fig. 5). Specifically, we simulated the cardiac responses to increased energy expenditure with *1*) activation of all pathways as in Fig. 1; *2*) activation of all pathways except glycolysis and glycogen breakdown; *3*) activation of all pathways except mitochondrial dehydrogenases; *4*) activation of all pathways except complex I; *5*) activation of all pathways except complex V; and *6*) activation of all pathways except transferring of $NADH-NAD^+$ and ATP-ADP between the cytosol and mitochondria (denoted as "communication" in Fig. 5).

Prevention of the activation of glycolysis resulted in a major reduction in the cytosolic redox and the phosphorylation potential but had more modest effects in the mitochondria (Fig. 5). Preventing the activation of glycolysis resulted in a decrease in the cytosolic and mitochondrial $NADH/NAD^+$ ratio when energy expenditure was increased instead of the increase that was observed with parallel activation (Fig. 5). There was a modest decrease in the ATP/ADP ratio in both compartments when the activation of glycolysis was prevented and a greater effect in the cytosol than in the mitochondria (Fig. 5). In addition, the steady-state $M\dot{V}O_2$ was decreased from 10.1 to 9.1 $\mu mol \cdot g^{-1} \cdot min^{-1}$ when activation of glycolysis was blocked (data not shown).

Blockade of the activation of mitochondrial dehydrogenases had profound effects on both mitochondrial and cytosolic redox, the phosphorylation potential, and the increase in $M\dot{V}O_2$, suggesting that this process is critical for maintaining metabolic homeostasis in the transition from normal to high rates of energy expenditure. Simulation results show that preventing the activation of mitochondrial dehydrogenases resulted in a ~50% decrease in both cytosolic and mitochondrial $NADH/NAD^+$ and ATP/ADP ratios (Fig. 5). The increase from baseline in steady-state $M\dot{V}O_2$ was reduced by 74% (4.6 $\mu mol \cdot g^{-1} \cdot min^{-1}$) when the activation of mitochondrial dehydrogenases was prevented.

Preventing the activation of complex I caused a large increase in the cytosolic and mitochondrial $NADH/NAD^+$ ratio, a 40% decrease in the mitochondrial ATP/ADP ratio, and a 57% reduction the increase from baseline in steady-state $M\dot{V}O_2$ (5.8 $\mu mol \cdot g^{-1} \cdot min^{-1}$). In contrast to blockade of the activation of dehydrogenases, preventing the activation of complex I caused modest fall in the cytosolic ATP/ADP ratio. Blocking the activation of complex V had minor effects on metabolic homeostasis (Fig. 5) and had no effect on the increase in $M\dot{V}O_2$ (data not shown). Blocking activation of complex V had little effect on the mitochondrial and cytosolic $NADH/NAD^+$ or ATP/ADP ratios compared with parallel activation, suggesting that this step is less important than activation of mitochondrial dehydrogenases or complex I for maintaining metabolic homeostasis during the transition for normal to high rates of energy expenditure.

The role of communication between the cytosol and mitochondrial was investigated by preventing the activation of the exchange of ATP − ADP, and NADH − NAD^+ between the cytosol and mitochondria. This resulted in a slight decrease in mitochondrial $NADH/NAD^+$ and a moderate decrease in cytosolic ATP/ADP but a huge increase in mitochondrial ATP/ADP ratio and cytosolic $NADH/NAD^+$. The steady-state increase in $M\dot{V}O_2$ was lowered by only 6% when the activation of the exchange of ATP − ADP and NADH − NAD^+ was prevented.

Effects of elevated arterial lactate. In silico experiments were performed to investigate the role of elevated arterial lactate concentration on cardiac metabolism during the transition from resting to increased energy expenditure conditions (Fig. 6). Simulations were performed with a constant arterial lactate concentration of 0.7 mM (as in Figs. 2–5) and with an increase in arterial lactate to either 2.1 or 4.2 mM (Fig. 6) to mimic the increases in arterial lactate observed in human exercise. Arterial lactate concentration had no effect on $M\dot{V}O_2$, the rate of oxidative phosphorylation, and the concentrations of ATP, ADP, or phosphocreatine (data not shown). Increased arterial lactate concentration increased pyruvate oxidation and reduced myocardial fatty acid oxidation (Fig. 6*C*). Cytosolic $NADH/NAD^+$ ratios (~40–90% at 2.1 mM and ~90%-140% at 4.2 mM) were increased as a function of elevations in arterial lactate concentration, reflecting a major effect on lactate uptake and the lactate dehydrogenase reaction (Fig. 6). On the other hand, the mitochondrial $NADH/NAD^+$ ratio was not affected significantly by elevated arterial lactate concentration during the first 5 min but was 10–15% higher with elevated

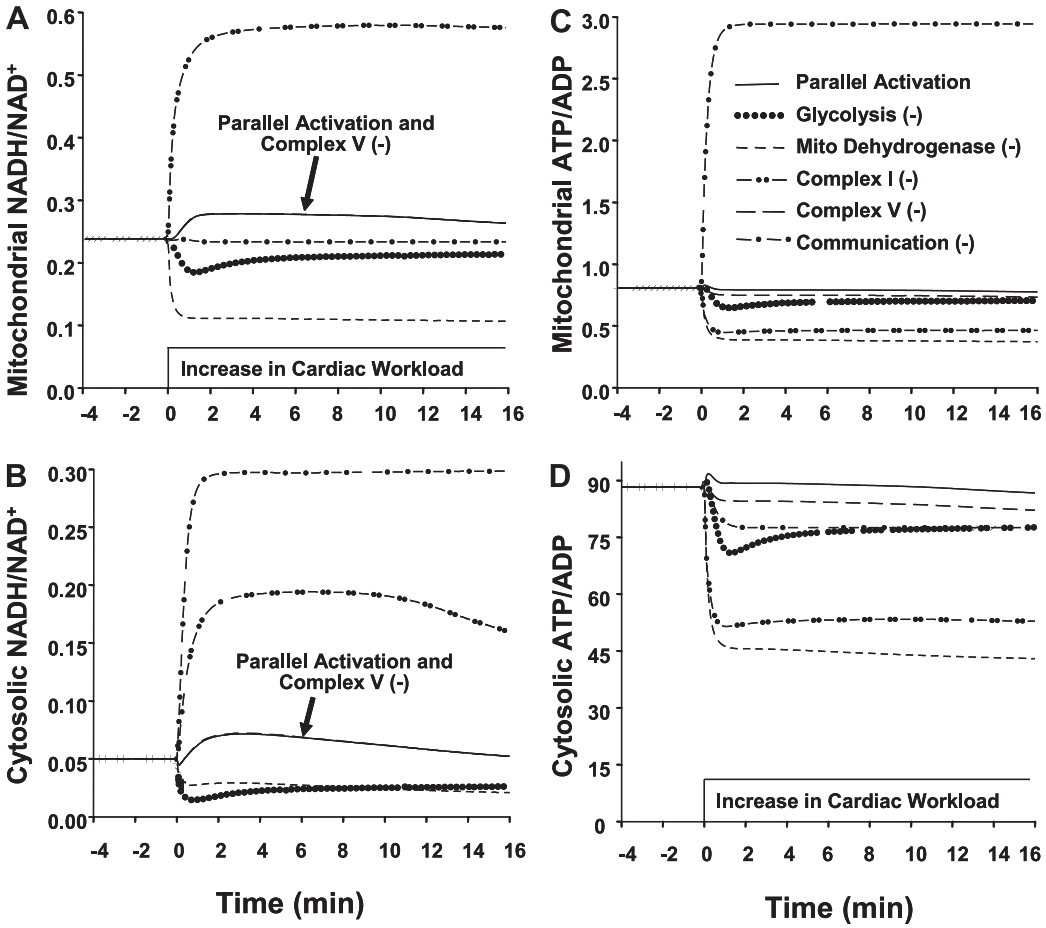

Fig. 5. Effects of pathway activation on metabolic homeostasis in response to increased energy expenditure. *A*: mitochondrial NADH/NAD$^+$; *B*: cytosolic NADH/NAD$^+$; *C*: mitochondrial ATP/ADP; *D*: cytosolic ATP/ADP.

arterial lactate at 16 min of increased work, reflecting a higher cytosolic NADH/NAD$^+$ ratio and elevated pyruvate oxidation compared with low arterial lactate concentrations.

Dynamic responses of diabetic heart to increased energy expenditure. Conditions in the diabetic myocardium were simulated by increasing the arterial concentrations of β-hydroxybutyrate from 0.03 to 0.8 mM and glucose from 4.75 to 9.5 mM and reducing the maximal velocities for glucose transport by 50% and PDH activity by 25% with normal energy expenditure (Fig. 7, *phase I*). There was a decrease in pyruvate oxidation (from 0.37 to 0.31 $\mu mol \cdot g^{-1} \cdot min^{-1}$) and a slight increase in fatty acids oxidation (from 0.07 to 0.078 $\mu mol \cdot g^{-1} \cdot min^{-1}$), and the heart began to utilize β-hydroxybutyrate as a fuel (Fig. 7). In response to a fourfold increase in energy expenditure, the peak value of pyruvate oxidation under diabetic conditions was 1.2 $\mu mol \cdot g^{-1} \cdot min^{-1}$, which was lower than that in the normal heart (1.9 $\mu mol \cdot g^{-1} \cdot min^{-1}$) (Fig. 7*B*, *phase II*). On the other hand, the rate of fatty acids oxidation under diabetic conditions was increased compared with the nondiabetic conditions (Fig. 7*C*), and β-hydroxybutyrate oxidation rate increased dramatically to 0.18 $\mu mol \cdot g^{-1} \cdot min^{-1}$ (Fig. 7*A*). Diabetes decreased the cytosolic NADH/NAD$^+$ ratio and had no effect on the mitochondrial NADH/NAD$^+$ ratio (Fig. 7*D*) nor on the rates of ATP generation or $M\dot{V}O_2$ (data not shown).

DISCUSSION

The results of the present investigation add further support to the concept that an abrupt increase in cardiac energy expenditure results in a simultaneous activation of metabolic processes in both cytosol (ATP hydrolysis, glycogen breakdown, and glycolysis) and mitochondria (dehydrogenase activity, NADH oxidation, oxidative phosphorylation of ADP) (4, 21, 28, 29, 43, 45). This parallel activation has been demonstrated to be essential for maintaining metabolic homeostasis (e.g., ATP, ADP, and Pi) in response to increased energy demand, as shown in Fig. 5, supporting previous findings by other investigators (3, 27). The results also show the novel finding of a transient increase in the NADH/NAD$^+$ ratio in both the cytosolic and mitochondrial compartments, with a peak increase of a 40% increase in the cytosol over baseline values but only a 20% increase in the mitochondria. On the other hand, we found that an elevation in arterial lactate concentration with the onset of the increase in energy expenditure increased the cytosolic NADH/NAD$^+$ ratio and mitochondrial pyruvate oxidation and reduced fatty acid oxidation but had little effect on the mitochondrial NADH/NAD$^+$ ratio. Finally, our simulation results under diabetic conditions showed that the dynamics of the mitochondrial NADH/NAD$^+$ ratio was not altered during increase energy expenditure despite enhanced oxidation of β-hy-

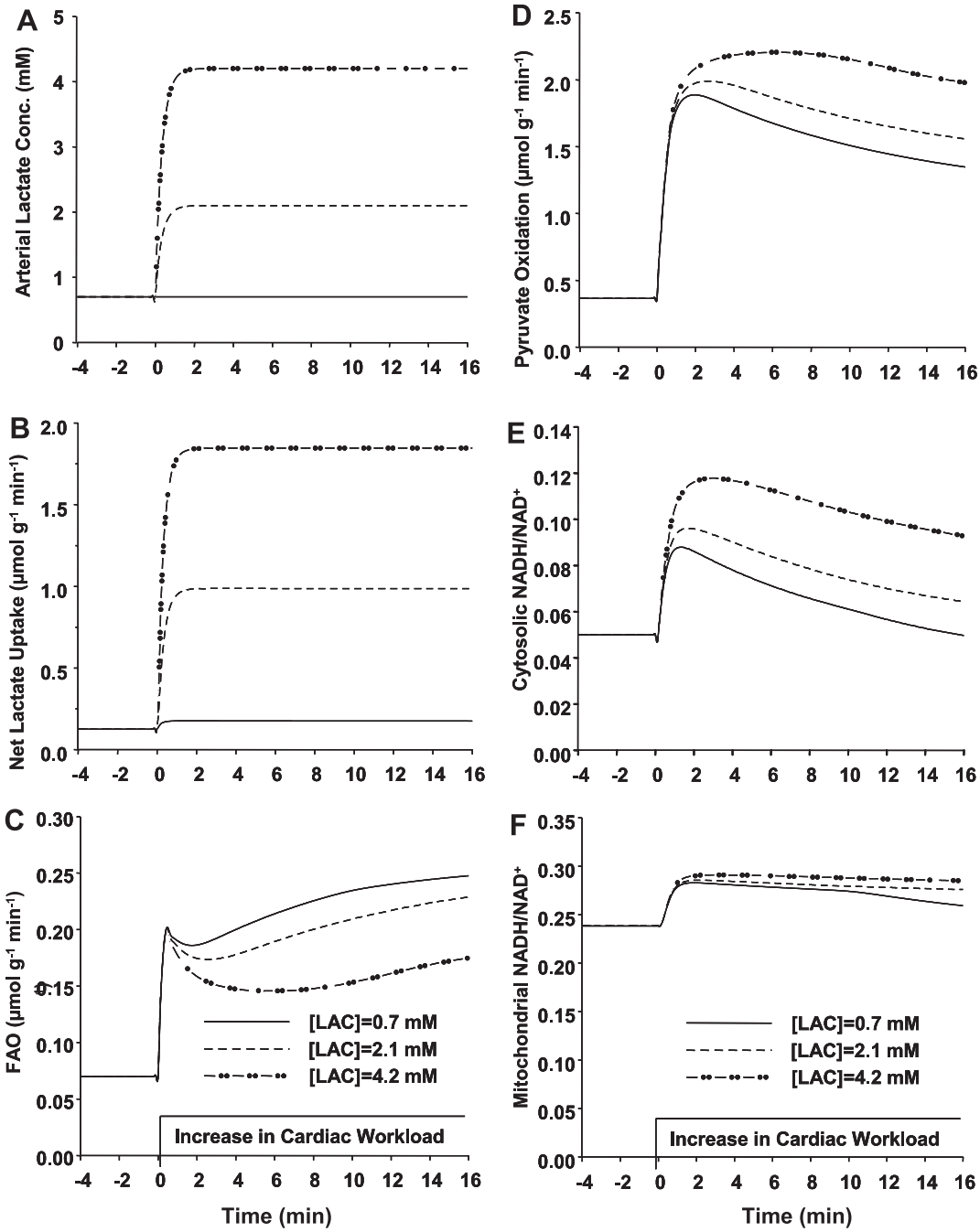

Fig. 6. Model simulated dynamics of arterial lactate (LAC) concentration (*A*), myocardial lactate uptake (*B*), fatty acid oxidation (*C*), pyruvate oxidation (*D*), cytosolic NADH/NAD^+ ratio (*E*), and mitochondrial NADH/NAD^+ (*F*) in response to increased energy expenditure.

droxybutyrate and fatty acids and reduced pyruvate oxidation. It is important to point out that in the present model, the total ATP+ADP+AMP and NADH+NAD^+ pools were conserved; however, there were no constraints to maintain constant ATP/ADP and NADH/NAD^+ ratios.

Model validation. The findings of the present study cannot be obtained using current experimental methods, which clearly demonstrates the utility of computational models in the investigation of the regulatory mechanism of cellular energy metabolism. We can, however, validate our computational model by comparing some of the simulation results with data we recently obtained in anesthetized pigs subjected to a fourfold increase in myocardial workload for 17 min (26, 36). Our model simulations corresponded closely with available experimental data on $M\dot{V}O_2$ (36) (Fig. 2*A*) and the concentrations of glycogen, lactate (Fig. 3*A*), tissue NADH, and NAD^+ (Fig. 4*C*). Accompanying the increased energy expenditure was an increase in pyruvate oxidation (4.7-fold) (Fig. 5*A*) and fatty acid oxidation (3.2-fold) (Fig. 2*C*), even in the absence of an increase in arterial lactate concentration, which is similar to the relative increase we previously measure for oxidation of exogenous glucose and fatty acids in pigs subjected to a three- to fourfold

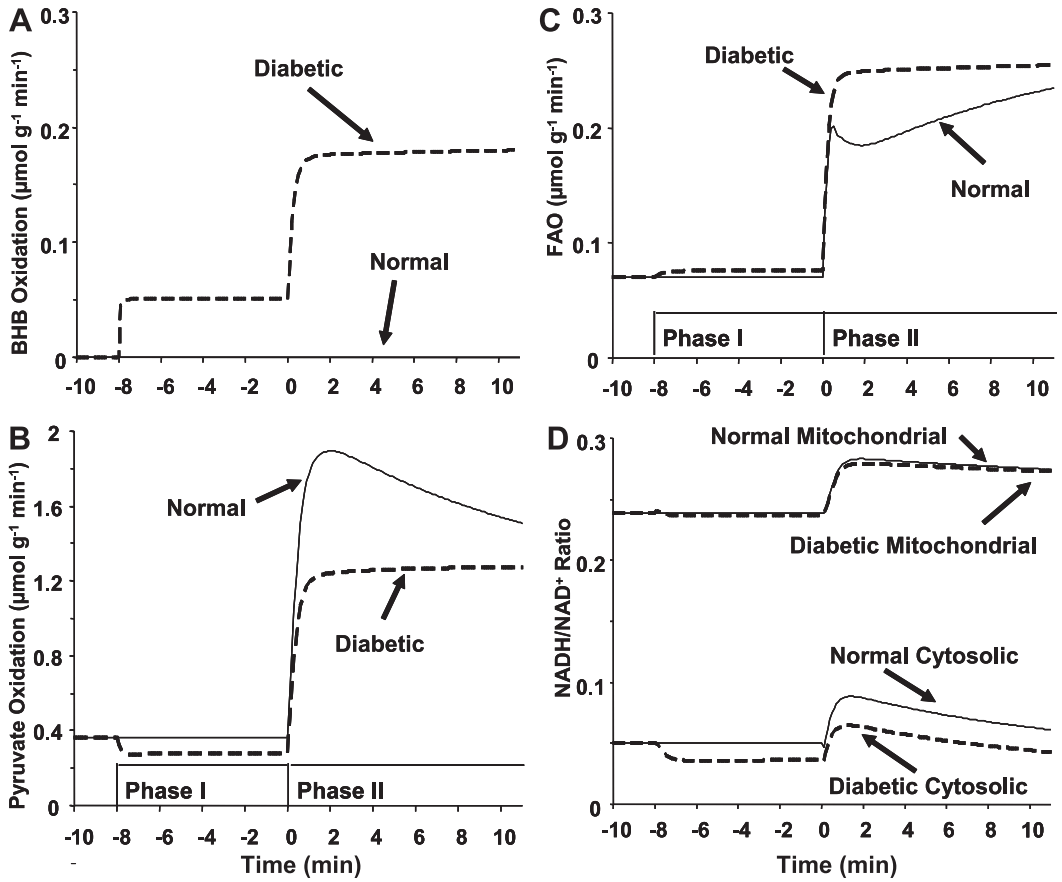

Fig. 7. Model simulated dynamics of β-hydroxybutyrate oxidation (*A*), pyruvate oxidation (*B*), fatty acid oxidation (*C*), and ATP generation (*D*). In *phase I*, metabolic conditions were altered to mimic conditions in the diabetic heart (e.g., high β-hydroxybutyrate + high glucose + inhibited glucose uptake, as described in the METHODS section). In *phase II* cardiac energy expenditure was increased as in Figs. 2–4.

increase in $M\dot{V}O_2$ (20, 26, 36). Thus the heart increases its reliance on carbohydrate oxidation with increased cardiac work, as demonstrated in previous experimental studies in humans and pigs (16, 30, 36) and in the isolated perfused rat heart (12, 17). Moreover, model simulations predicted a greater rate of lactate uptake and pyruvate oxidation as a function of increased arterial lactate concentration, which resulted in inhibition of fatty acid oxidation. The greater rate of pyruvate oxidation with elevated lactate corresponded with an increase in the cytosolic NADH/NAD^+ ratio, without significant effect on the mitochondrial NADH/NAD^+ ratio (Fig. 6), suggesting that alterations in mitochondrial NADH/NAD^+ are not essential for lactate inhibition of fatty acid oxidation at high rates of energy expenditure.

Parallel activation of metabolic pathways in response to increased energy expenditure. There is growing evidence that the fine regulation of myocardial ATP concentration during the transition from resting conditions to increased cardiac workload is due to the parallel activation of multiple metabolic steps concomitant with the increase in contractile power and ATP hydrolysis (28, 29). ATP formation is driven by the activity of complex V, availability of ADP and Pi, the proton motive force across the mitochondrial inner membrane, the activity of the complexes of the ETC, and the delivery of reducing equivalents (NADH and FADH2) to complexes I and II. The results of the present investigation are consistent with evidence from previous experimental studies (3, 4, 6, 34, 44) and computational models (28, 29). The mechanisms for the parallel activation remains somewhat unclear but can be at least partially attributed to Ca^{2+} activation of glycolysis, mitochondrial dehydrogenases, and complex V (31, 34, 42, 44). One possible signaling source between aerobic metabolism and myocardial work is Ca^{2+} (3) because it not only regulates myosin ATPase and sarcoplasmic reticulum Ca^{2+}-ATPase but also directly regulates cytosolic ATP hydrolysis, mitochondrial dehydrogenases (3, 6, 31, 43, 44), and complex V (34, 43). Furthermore, in vitro studies show that Ca^{2+} can also activate PDH phosphatase (therefore activates PDH) and the tricarboxylic acid cycle enzymes isocitrate dehydrogenase and α-ketoglutarate dehydrogenase, stimulating NADH generation (31). Moreover, it has been demonstrated that there is an increase in mitochondrial Ca^{2+} when there is an increase in extramitochondrial Ca^{2+}, such as that occurs with adrenergic stimulation (31). An additional activator is an increase in free Pi, which can activate complex I and oxidative phosphorylation during the transition to high rates of energy expenditure (6). Another possibility is that there is direct allosteric activation of complex I, as suggested by the observation that complex I in heart mitochondria is phosphorylated in a cAMP-dependent manner (11).

To investigate quantitatively the extent of control exerted by various components of "parallel activation" in maintaining the metabolic homeostasis observed in the present study and other

experimental studies, we simulated the cardiac responses to increased energy expenditure without activation of specific pathways (Fig. 5). We found that only when all the components of "parallel activation" investigated were activated simultaneously and to the same extent, the ADP and ATP concentration in both cytosol and mitochondria remained nearly constant. Without activating glycolysis and mitochondrial dehydrogenases, the NADH/NAD^+ ratios in both cytosol and mitochondria decreased, which makes sense because these pathways are the major producers of reducing equivalents. This also decreased the ATP/ADP ratio in the cytosol and mitochondria because, as we discussed above, mitochondrial ATP resynthesis relies on a steady-state supply of reducing equivalents. Hindrance of complex I blocked the consumption of NADH causing an increase in NADH and a decrease in ATP due to lowering the H^+ gradient across the inner mitochondrial membrane and inhibiting ATP synthesis (Fig. 5, *C* and *D*). Activation of complex V did not affect the NADH/NAD^+ and ATP/ADP ratios significantly, indicating that this component is not the key site for the regulation of metabolic homeostasis under these conditions. Whereas we have found that with ischemia the metabolic communication between cytosol and mitochondria is impaired (47), in the present investigation we show that active metabolic communication is essential for maintaining constant concentrations of energy transfer species during the transition from normal condition to increased energy expenditure. Without the transferring systems activated, mitochondrial ATP/ADP increased significantly, whereas cytosolic ATP/ADP decreased. This is not surprising, considering that more than 96% of ATP is produced inside the mitochondria, whereas almost all ATP is hydrolyzed inside the cytosol to support cardiomyocytes contraction. From these results, we concluded that *1*) mitochondrial ATP/ADP and cytosolic NADH/NAD^+ are mostly affected by the transferring of ATP-ADP and NADH-NAD^+, *2*) mitochondrial NADH/NAD^+ is mainly regulated by complex I and mitochondrial dehydrogenases, and *3*) cytosolic ATP/ADP is regulated by both mitochondrial dehydrogenases and complex I.

Substrate selection in diabetic heart in response to increased energy expenditure. One established feature of the diabetic heart is altered myocardial substrate utilization [e.g., increased fatty acids and/or ketone body utilization, and decreased glucose uptake and pyruvate oxidation, and utilization (41)]; however, the effect of increased workload on substrate metabolism and the corresponding regulatory mechanism in diabetic hearts are not well understood. We observed enhanced β-hydroxybutyrate and fatty acids oxidation and depressed pyruvate oxidation under conditions of increased energy expenditure (Fig. 7). Previous studies in diabetic hearts show reduced PDH activity and pyruvate oxidation, greater ketone body oxidation, and normal or enhanced fatty acid oxidation (1, 10, 14, 18). The results of the present investigation provide evidence that impaired pyruvate oxidation in the diabetic heart is not due to an increase in mitochondrial NADH/NAD^+ (Fig. 7), as previously suggested by measurements in isolated mitochondria from diabetics rats (24).

Model limitations and future directions. Whereas the current model is able to predict the cardiac responses to increased energy expenditure and provide useful insight into metabolic regulatory mechanism, there are several limitations that need to be addressed. The present model does not link substrate metabolism and ATP hydrolysis with mechanical power generation, cardiac myocytes extraction-contraction coupling, and Ca^{2+} transients. Incorporation of mechanical power generation would allow for the evaluation of mechanical efficiency of cardiac muscle during increased energy expenditure. Although the model has included a multistep activation mechanism, the activation was implemented in the model by increasing the rate coefficients and not through a direct link to the dynamics of Ca^{2+} in the cytosol and mitochondria in response to increased workload. Finally, the experimental validation data does not provide the dynamic information during the transition to increased energy expenditure. Model simulation shows that at the very beginning of increased workload, the cytosolic and mitochondrial NADH and NAD^+ are slightly changed, which may be caused by the activation of glycogen breakdown and the increased NADH generation from pyruvate and fatty acid oxidation. Additional experimental studies are needed to validate these transient dynamics. Finally, a systematic sensitivity analysis is needed to quantitatively analyze the effect of each reaction or transport process on the dynamics of metabolites in response to metabolic stress.

In summary, our in silico studies suggest that with the onset of an abrupt increase in cardiac energy expenditure there is a parallel activation of glycolysis, pyruvate oxidation, fatty acid oxidation, and ATP generation, resulting in constant concentrations of ATP and ADP in the cytosol and mitochondria. On the other hand, we observed that both cytosolic and mitochondrial NADH/NAD^+ increased during the first minutes (by 40% and 20%, respectively) and returned to the resting values by 15 min. Furthermore, model simulations showed that an elevation in arterial lactate concentration greatly increased the cytosolic NADH/NAD^+ ratio but had a lesser effect on the mitochondrial NADH/NAD^+ ratio. On the other hand, simulation of diabetic conditions reduced pyruvate oxidation and the cytosolic NADH/NAD^+ ratio but did not effect mitochondrial NADH/NAD^+ ratio, illustrating that alterations in mitochondrial substrate selection can occur independent of large changes in the mitochondrial NADH/NAD^+ ratio.

ACKNOWLEDGMENTS

This work was support by National Institutes of Health (NIH) Grant GM-66309 that established the Center for Modeling Integrated Metabolic Systems (MIMS) and by NIH Grant HL-074237. N. Sharma was supported by a predoctoral fellowship from the American Heart Association, Ohio Valley Affiliate.

REFERENCES

1. **Avogaro A, Nosadini R, Doria A, Fioretto P, Velussi M, Vigorito C, Sacca L, Toffolo G, Cobelli C, and Trevisan R.** Myocardial metabolism in insulin-deficient diabetic humans without coronary artery disease. *Am J Physiol Endocrinol Metab* 258: E606–E618, 1990.
2. **Balaban RS.** Regulation of oxidative phosphorylation in the mammalian cell. *Am J Physiol Cell Physiol* 258: C377–C389, 1990.
3. **Balaban RS, Bose S, French SA, and Territo PR.** Role of calcium in metabolic signaling between cardiac sarcoplasmic reticulum and mitochondria in vitro. *Am J Physiol Cell Physiol* 284: C285–C293, 2003.
4. **Balaban RS, Kantor HL, Katz LA, and Briggs RW.** Relation between work and phosphate metabolite in the in vivo paced mammalian heart. *Science* 232: 1121–1123, 1986.
5. **Beard DA.** A biophysical model of the mitochondrial respiratory system and oxidative phosphorylation. *PLoS Comput Biol* 1: e36, 2005.
6. **Bose S, French S, Evans FJ, Joubert F, and Balaban RS.** Metabolic network control of oxidative phosphorylation: multiple roles of inorganic phosphate. *J Biol Chem* 278: 39155–39165, 2003.

7. **Bunger R, Permanetter B, and Yaffe S.** Energy utilization and pyruvate as determinants of pyruvate dehydrogenase in norepinephrine-stimulated heart. *Pflügers Arch* 397: 214–219, 1983.
8. **Cabrera ME, Zhou L, Stanley WC, and Saidel GM.** Regulation of cardiac energetics: role of redox state and cellular compartmentation during ischemia. *Ann NY Acad Sci* 1047: 259–270, 2005.
9. **Chance B and Williams GR.** The respiratory chain and oxidative phosphorylation. *Adv Enzymol Relat Subj Biochem* 17: 65–134, 1956.
10. **Chatham JC, Gao ZP, Bonen A, and Forder JR.** Preferential inhibition of lactate oxidation relative to glucose oxidation in the rat heart following diabetes. *Cardiovasc Res* 43: 96–106, 1999.
11. **Chen R, Fearnley IM, Peak-Chew SY, and Walker JE.** The phosphorylation of subunits of complex I from bovine heart mitochondria. *J Biol Chem* 279: 26036–26045, 2004.
12. **Collins-Nakai RL, Noseworthy D, and Lopaschuk GD.** Epinephrine increases ATP production in hearts by preferentially increasing glucose metabolism. *Am J Physiol Heart Circ Physiol* 267: H1862–H1871, 1994.
13. **Cortassa S, Aon MA, Marban E, Winslow RL, and O'Rourke B.** An integrated model of cardiac mitochondrial energy metabolism and calcium dynamics. *Biophys J* 84: 2734–2755, 2003.
14. **Doria A, Nosadini R, Avogaro A, Fioretto P, and Crepaldi G.** Myocardial metabolism in type 1 diabetic patients without coronary artery disease. *Diabet Med* 8: S104–S107, 1991.
15. **Forsey RG, Reid K, and Brosnan JT.** Competition between fatty acids and carbohydrate or ketone bodies as metabolic fuels for the isolated perfused heart. *Can J Physiol Pharmacol* 65: 401–406, 1987.
16. **Gertz EW, Wisneski JA, Stanley WC, and Neese RA.** Myocardial substrate utilization during exercise in humans dual carbon-labeled carbohydrate isotope experiments. *J Clin Invest* 82: 2017–2025, 1988.
17. **Goodwin GW, Taylor CS, and Taegtmeyer H.** Regulation of energy metabolism of the heart during acute increase in heart work. *J Biol Chem* 273: 29530–29539, 1998.
18. **Hall JL, Lopaschuk GD, Barr A, Bringas J, Pizzurro RD, and Stanley WC.** Increased cardiac fatty acid uptake with dobutamine infusion in swine is accompanied by a decrease in maloanyl CoA levels. *Circ Res* 32: 879–885, 1996.
19. **Hall JL, Stanley WC, Lopaschuk GD, Wisneski JA, Pizzurro RD, Hamilton CD, and McCormack JG.** Impaired pyruvate osidation but normal glucose uptake in diabetic pig heart during dobutamine induced work. *Am J Physiol Heart Circ Physiol* 271: H2320–H2329, 1996.
20. **Hall JL, Van Wylen DG, Pizzurro RD, Hamilton CD, Reiling CM, and Stanley WC.** Myocardial interstitial purine metabolites and lactate with increased work in swine. *Cardiovasc Res* 30: 351–356, 1995.
21. **Heineman FW and Balaban RS.** Control of mitochondrial respiration in the heart in vivo. *Annu Rev Physiol* 52: 523–542, 1990.
22. **Heineman FW and Balaban RS.** Effects of afterload and heart rate on NAD(P)H redox state in the isolated rabbit heart. *Am J Physiol Heart Circ Physiol* 264: H433–H440, 1993.
23. **Heiss HW, Barmeyer J, Wink K, Hell G, Cerny FJ, Keul J, and Reindell H.** Studies on the regulation of myocardial blood flow in man. I: Training effects on blood flow and metabolism of the healthy heart at rest and during standardized heavy exercise. *Basic Res Cardiol* 71: 658–675, 1976.
24. **Kerbey AL, Radcliffe PM, and Randle PJ.** Diabetes and the control of pyruvate dehydrogenase in rat heart mitochondria by concentration ratios of adenosine triphosphate/adenosine diphosphate, of reduced/oxidized nicotinamide-adenine dinucleotide and of acetyl-coenzyme A/coenzyme A. *Biochem J* 164: 509–519, 1977.
25. **Khouri EM, Gregg DE, and Rayford CR.** Effect of exercise on cardiac output, left coronary flow and myocardial metabolism in the unanesthetized dog. *Circ Res* 17: 427–437, 1965.
26. **King KL, Okere IC, Sharma N, Dyck JR, Reszko AE, McElfresh TA, Kerner J, Chandler MP, Lopaschuk GD, and Stanley WC.** Regulation of cardiac malonyl-CoA content and fatty acid oxidation during increased cardiac power. *Am J Physiol Heart Circ Physiol* 289: H1033–H1037, 2005.
27. **Korzeniewski B.** Regulation of ATP supply in mammalian skeletal muscle during resting state–intensive work transition. *Biophys Chem* 83: 19–34, 2000.
28. **Korzeniewski B.** Regulation of oxidative phosphorylation in different muscles and various experimental conditions. *Biochem J* 375: 799–804, 2003.
29. **Korzeniewski B, Noma A, and Matsuoka S.** Regulation of oxidative phosphorylation in intact mammalian heart in vivo. *Biophys Chem* 116: 145–157, 2005.
30. **Massie BM, Schwartz GG, Garcia J, Wisneski JA, Weiner MW, and Owens T.** Myocardial metabolism during increased work states in the porcine left ventricle in vivo. *Circ Res* 74: 64–73, 1994.
31. **McCormack JG, Halestrap AP, and Denton RM.** Role of calcium ions in regulation of mammalian intramitochondrial metabolism. *Physiol Rev* 70: 391–425, 1990.
32. **Newsholme EA and Randle PJ.** Regulation of glucose uptake by muscle. Effects of fatty acids, ketone bodies and pyruvate, and of alloxan-diabetes, starvation, hypophysectomy and adrenalectomy, on the concentrations of hexose phosphates, nucleotides and inorganic phosphate in perfused rat heart. *Biochem J* 93: 641–651, 1964.
33. **Randle PJ.** Fuel selection in animals. *Biochim Soc Trans* 14: 799–806, 1986.
34. **Scholz TD and Balaban RS.** Mitochondrial F1-ATPase activity of canine myocardium: effects of hypoxia and stimulation. *Am J Physiol Heart Circ Physiol* 266: H2396–H2403, 1994.
35. **Sharma N and Stanley WC.** Power and control: transferring energy when there is work to be done. *Physiology* 59: 29–30, 2005.
36. **Sharma N, Okere IC, Brunengraber DZ, McElfresh TA, King KL, Sterk JP, Huang H, Chandler MP, and Stanley WC.** Regulation of pyruvate dehydrogenase activity and citric acid cycle intermediates during high cardiac power generation. *J Physiol* 562: 593–603, 2005.
37. **Spitzer JJ.** Effect of lactate infusion on canine myocardial free fatty acid metabolism in vivo. *Am J Physiol* 226: 213–217, 1974.
38. **Stanley WC.** Myocardial lactate metabolism during exercise. *Med Sci Sports Exerc* 23: 920–924, 1991.
39. **Stanley WC, Gertz EW, Wisneski JA, Morris DL, Neese RA, and Brooks GA.** Systemic lactate kinetics during graded exercise in man. *Am J Physiol Endocrinol Metab* 249: E595–E602, 1985.
40. **Stanley WC, Lopaschuk GD, and McCormack JG.** Regulation of energy substrate metabolism in the diabetic heart. *Cardiovasc Res* 34: 25–33, 1997.
41. **Stanley WC, Meadows SR, Kivilo KM, Roth BA, and Lopaschuk GD.** β-Hydroxybutyrate inhibits myocardial fatty acid oxidation in vivo independent of changes in malonyl-CoA content. *Am J Physiol Heart Circ Physiol* 285: H1626–H1631, 2003.
42. **Stanley WC, Recchia FA, and Lopaschuk GD.** Myocardial substrate metabolism in the normal and failing heart. *Physiol Rev* 85: 1093–1129, 2005.
43. **Territo PR, French SA, and Balaban RS.** Simulation of cardiac work transitions, in vitro: effects of simultaneous Ca2+ and ATPase additions on isolated porcine heart mitochondria. *Cell Calcium* 30: 19–27, 2001.
44. **Territo PR, Mootha VK, French SA, and Balaban RS.** Ca^{2+} activation of heart mitochondrial oxidative phosphorylation: role of the F(0)/F(1)-ATPase. *Am J Physiol Cell Physiol* 278: C423–C435, 2000.
45. **Wan B, Doumen C, Duszynski J, Salama G, Vary TC, and LaNoue KF.** Effects of cardiac work on electrical potential gradient across mitochondrial membrane in perfused rat hearts. *Am J Physiol Heart Circ Physiol* 265: H453–H460, 1993.
46. **Zhou L, Salem JE, Saidel GM, Stanley WC, and Cabrera ME.** Mechanistic model of cardiac energy metabolism predicts localization of glycolysis to cytosolic subdomain during ischemia. *Am J Physiol Heart Circ Physiol* 288: H2400–H2411, 2005.
47. **Zhou L, Stanley WC, Saidel GM, Yu X, and Cabrera ME.** Regulation of lactate production at the onset of ischaemia is independent of mitochondrial NADH/NAD+: insights from in silico studies. *J Physiol* 569: 925–937, 2005.